J Mater Sci (2011) 46:2410–2421
DOI 10.1007/s10853-010-5087-y

# Diffusion-induced recrystallization in the Cu(Pd) system at complete solid-solution temperatures

**S. Inomata · M. O · M. Kajihara**

Received: 21 April 2010 / Accepted: 15 November 2010 / Published online: 2 December 2010


**Abstract** Owing to annealing at complete solid-solution temperatures around 1,000 K, Pd can quickly penetrate into Cu due to diffusion-induced recrystallization (DIR). To examine this penetration behavior, DIR in the Cu(Pd) system was experimentally observed in the present study. A diffusion bonding technique was used to prepare polycrystalline Cu/Pd/Cu diffusion couples. The diffusion couple was isothermally annealed at temperatures of $T = 923$–$1{,}023$ K for various times up to $t = 176$ h. During annealing, a region alloyed with Pd is produced in Cu from the Cu/Pd interface due to DIR. The concentration of Pd on the Pd-rich side in the DIR region remains almost constant independent of the annealing time but increases with increasing annealing temperature. On the other hand, the mean thickness of the DIR region increases with increasing annealing time. The growth rate of the DIR region is a monotonically increasing function of the annealing temperature. The experimental findings of the kinetics study were quantitatively analyzed using a mathematical model. The analysis satisfactorily reproduces the overall growth behavior of the DIR region.

## Introduction

Diffusion-induced recrystallization (DIR) and diffusion-induced grain-boundary migration (DIGM) are known to occur in many binary alloys [1–3]. DIR is the phenomenon that new fine grains with discontinuously different solute concentrations are formed behind moving grain boundaries owing to recrystallization combined with diffusion of solute atoms along the moving and stationary boundaries surrounding the fine grains. In contrast, during DIGM, a region with different composition is left behind a moving boundary due to grain boundary migration combined with the diffusion of solute atoms along the moving boundary.

In the binary Cu–Ni system, a complete solid-solution phase with the face-centered cubic (fcc) structure is stable in the temperature range between 628 and 1,358 K [4]. If a diffusion couple consisting of Cu and Ni is annealed in this temperature range, the interdiffusion between Cu and Ni may take place across the Cu/Ni interface due to volume diffusion. At low annealing temperatures, however, the volume diffusion in the fcc phase is negligible and thus practically frozen out. Even under such conditions, penetration of Ni into Cu may be accelerated by DIR and/or DIGM [5–14]. DIGM and DIR in the Cu(Ni) and Ni(Cu) systems were experimentally studied by various researchers using Cu/Ni/Cu diffusion couples prepared by an electrodeposition technique [5–7]. In these experiments, the diffusion couple was isothermally annealed at temperatures of 623–1,223 K. After annealing, the morphology near the Cu/Ni interface region exhibited both DIGM and DIR characteristics, whereas only DIGM was observed in both the Cu and Ni matrices slightly away from the interface. Though the kinetics of DIGM was examined from the microstructural observation of the DIGM area, it was rather difficult to distinguish the region alloyed by DIR from that alloyed by DIGM. Hence, the growth behavior of the DIR region was not determined in these experiments.

Many defects will be present in a polycrystalline Cu layer electrodeposited onto Ni. Such defects may be responsible for the mixed DIGM and DIR morphology in

S. Inomata · M. O
Graduate School, Tokyo Institute of Technology, Yokohama 226-8502, Japan

M. Kajihara (✉)
Department of Materials Science and Engineering, Tokyo Institute of Technology, Yokohama 226-8502, Japan
e-mail: kajihara@materia.titech.ac.jp

the near-interface region. Previously [8, 9, 14], Cu/Ni/Cu diffusion couples were prepared to suppress this defect formation by diffusion bonding Cu and Ni. In these studies, the diffusion couple was isothermally annealed at temperatures of 723–1,023 K to observe the kinetics of DIR in the Cu(Ni) and Ni(Cu) systems. The resulting DIR region at the Cu/Ni interface was clearly recognized, and no mixed DIGM + DIR region was formed in the diffusion couple. Therefore, the diffusion bonding technique rather than the electrodeposition technique is more suitable for the preparation of diffusion couples in DIR studies.

Like the binary Cu–Ni system [4], a complete solid-solution fcc phase is stable at temperatures of 871–1,358 K in the binary Cu–Pd system [15]. The interdiffusion in the binary Cu–Pd system has been experimentally studied by many investigators [16–20]. In the experiment by Nakahara et al. [16], polycrystalline Cu/Pd diffusion couples with very fine grains were prepared by the electrodeposition technique and then observed by transmission electron microscopy (TEM). The TEM observation indicates that DIGM occurs in Pd of the diffusion couple even at room temperature. Also in the experiment by Chow et al. [17], the electrodeposition technique was used to prepare polycrystalline Cu/Pd diffusion couples. In their experiment, however, the diffusion couple was isothermally annealed at temperatures of 573–973 K. During annealing, fast penetration of Pd into Cu takes place due to boundary diffusion. Such boundary diffusion was observed also by Bukaluk [18] and Chakraborty et al. [20]. Since the fast penetration is controlled by boundary diffusion, DIR as well as DIGM may occur in the Cu–Pd system. Although DIGM was reported by Nakahara et al. [16], obtainable information is limited for DIR. In order to examine whether DIR actually takes place in the Cu–Pd system, Cu/Pd/Cu diffusion couples were prepared by the diffusion bonding technique and then isothermally annealed at complete solid-solution temperatures of 923–1,023 K in the present study. The microstructure of the annealed diffusion couple was observed in a metallographical manner. The observation was quantitatively analyzed using the mathematical models proposed in previous studies [21, 22].

## Experimental

Plate specimens of pure Cu with a dimension of 12 × 5 × 1.5 mm were cut from a commercial plate of pure Cu with purity of 99.96% and a size of 100 × 100 × 1.5 mm and then separately annealed in evacuated silica capsules at 1,173 K for 2 h, followed by air cooling without breaking the capsules. The two surfaces with an area of 12 × 5 mm of each annealed Cu plate specimen were mechanically polished on 400–4000 emery papers until a depth of 100 μm and then finished using diamond with a diameter of 1 μm. After mechanical polishing, the pure Cu plate specimen was electrolytically polished with a cathode of an austenitic stainless steel in an etchant consisting of 20 vol.% of nitric acid and 80 vol.% of methanol at a voltage of 6 V for 180 s at 238 K.

Sheet specimens of pure Pd with a dimension of 14 × 7 × 0.1 mm were prepared by cold rolling and cutting from a commercial sheet of pure Pd with purity of 99.95% and a size of 50 × 50 × 0.5 mm and then separately annealed in evacuated silica capsules at 1,173 K for 3 h, followed by air cooling without breaking the capsules. The annealed Pd sheet specimen was chemically polished in nitrohydrochloric acid.

After chemical polishing, a Pd sheet specimen was immediately sandwiched between the finished surfaces of two freshly prepared Cu plate specimens in ethanol by the technique used in previous studies [10–12]. The Cu/Pd/Cu couple was completely dried and then isothermally heat-treated for diffusion bonding in an evacuated silica tube, followed by air cooling. The diffusion bonding was carried out at temperatures of 923, 973, and 1,023 K for times of 31, 24, and 17 h, respectively. The diffusion couples were separately encapsulated in evacuated silica capsules and then isothermally annealed at 923, 973, and 1,023 K for various periods up to 152 h. Hereafter, the annealing temperature is denoted by $T$, and the summation of the heat-treating and annealing times is merely called the annealing time $t$. Cross-sections of the annealed diffusion couple were mechanically polished using 1000-4000 emery papers and diamond with a size of 1 μm and then finished with an OP-S liquid manufactured by Struers Ltd.

The finished cross-section was chemically etched in two different etchants. The first one is composed of 12 mL of 25% aqua ammonia, 2.6 mL of 30% oxygenated water and 28 mL of distilled water, and the second one consists of 12 mL of acetic acid, 8 mL of nitric acid, five drops of hydrochloric acid and five drops of phosphoric acid. The chemical etchings with the former and latter etchants are called Etchings A and B, respectively. Both Etchings A and B were carried out for 2 s using the freshly prepared etchants. The microstructure of the cross-section was observed with a differential interference contrast optical microscope (DICOM). Concentration profiles of Cu and Pd on the cross-section were measured by electron probe microanalysis (EPMA).

## Results

### Microstructure

Typical DICOM photographs of the cross-sections with Etchings A and B for the diffusion couple annealed at

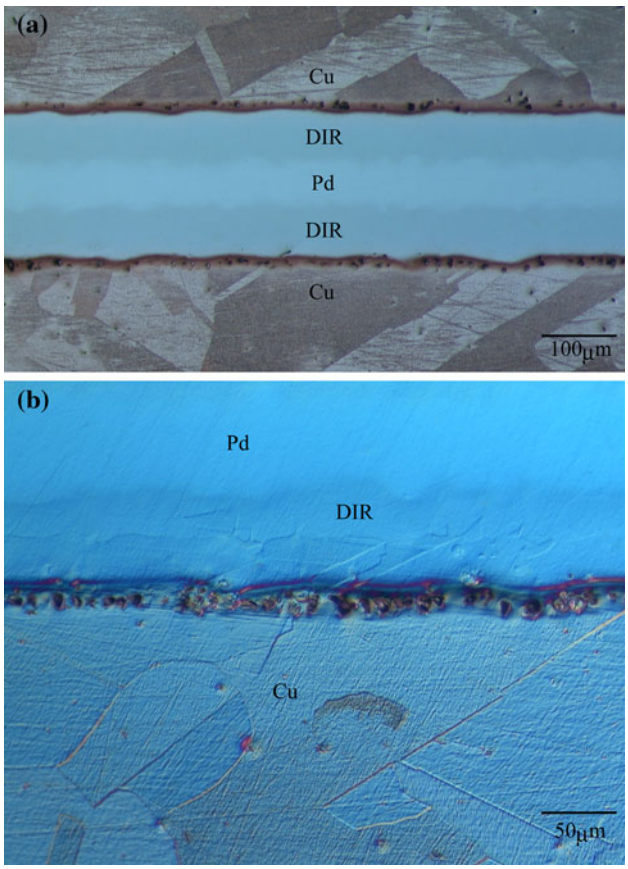


**Fig. 1** DICOM photographs of cross-sections of the Cu/Pd/Cu diffusion couple annealed at $T = 1{,}023$ K for $t = 70.02$ h (252.1 ks): **a** Etching A and **b** Etching B

$T = 1{,}023$ K for $t = 70.02$ h (252.1 ks) are shown in Fig. 1a and b, respectively. In Fig. 1a, the horizontal band with a thickness of about 60 μm is the pure Pd specimen, and the areas on the upper and lower sides of the Pd are the pure Cu specimens. On the other hand, a region with a slightly dark contrast and a thickness of about 70 μm is formed by DIR at each Cu/Pd interface. This slightly dark region produced by DIR is hereafter denominated the DIR region. The thickness of the Pd is initially about 100 μm but about 60 μm in Fig. 1a. Thus, in Fig. 1a, each side of the Pd is consumed by about 20 μm in thickness due to formation of the DIR region. However, the thickness of the DIR region is about 70 μm as mentioned above. This means that the DIR region rather predominantly grows into the Cu. Such growth behavior of the DIR region was observed at $T = 923$–$1{,}023$ K. Although the polycrystalline microstructure of the DIR region is invisible in Fig. 1a, it becomes visible in Fig. 1b. As can be seen in Fig. 1b, the mean grain size is much smaller for the DIR region than for the Cu. In Fig. 1a and b, many voids are observed in the Cu ahead of the DIR region. These voids may be formed at invisible Kirkendall voids by the chemical etching. The number of visible voids per unit area is larger in Fig. 1b than in Fig. 1a, even though Fig. 1a and b shows the cross-sections of the identical diffusion couple. Hence, the formation of visible voids is more remarkable for Etching B than for Etching A.

## Concentration profile

Concentration profiles of Cu and Pd across the DIR region were determined by EPMA. A typical result for the diffusion couple of Fig. 1 is shown as open circles in Fig. 2. Figure 2a indicates the whole concentration profile, and Fig. 2b shows the concentration profile magnified around the boundary between the DIR region and the Cu. In Fig. 2, the ordinate indicates the mole fraction $y$ of Pd, and the abscissa shows the distance $x$ along the direction normal to the initial Cu/Pd interface. As can be seen in Fig. 2a, the DIR region grows to a thickness of about 70 μm. Hereafter, the boundary between the DIR region and the Pd is called the Pd boundary, and that between the DIR region and the Cu is designated the Cu boundary. According to the result in Fig. 2, the chemical composition discontinuously changes across the Pd and Cu boundaries. This compositional

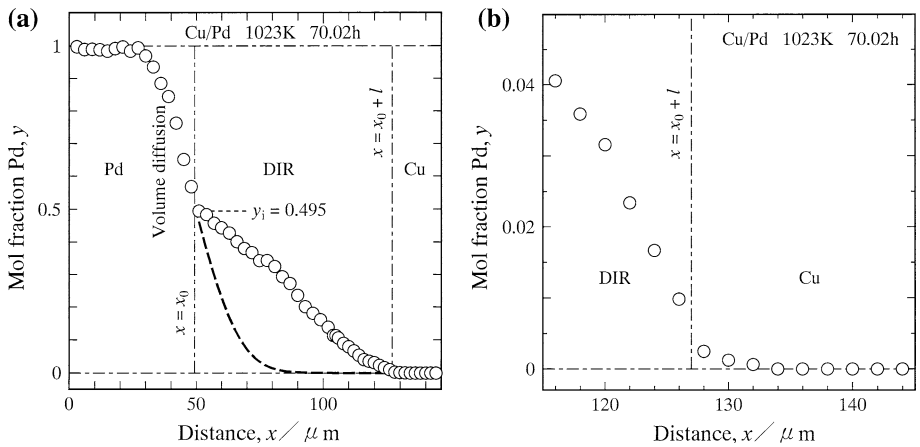


**Fig. 2** Concentration profiles of Pd in the Cu/Pd/Cu diffusion couple shown in Fig. 1 across **a** the DIR region and **b** the Cu boundary

discontinuity causes the contrast of the DIR region on the DICOM photographs in Fig. 1. As shown in Fig. 2, however, the absolute value of the compositional discontinuity is smaller for the Cu boundary than for the Pd boundary. Nevertheless, on the DICOM photographs in Fig. 1, the Cu boundary is more distinguishable than the Pd boundary. In the DIR region, the concentration of Pd monotonically decreases from $y = 0.495$ to $y = 0.010$ with increasing distance from $x = 51$ to $x = 126$ μm.

If the interdiffusion coefficient $D$ and the molar volume $V_m$ are both constant and independent of composition at a constant temperature, $y$ is expressed as an explicit function of $x$ and $t$ at $x > x_0$ by the following equation for the penetration of Pd into the Cu-rich fcc phase due to volume diffusion [23]:

$$y = y_i - (y_i - y_0)\mathrm{erf}\left(\frac{x - x_0}{2\sqrt{Dt}}\right). \quad (1)$$

Here, $x_0$ is the position of the Pd boundary, $y_0$ is the initial concentration of Pd in the Cu, and $y_i$ is the concentration of Pd in the DIR region at the Pd boundary. For the Cu/Pd/Cu diffusion couple, $y_0 = 0$. In Eq. 1, it is assumed that the Pd boundary is stationary and $y_i$ is constant independent of $t$. In a wide range of $y$, however, $D$ may vary depending on $y$. The dependence of $D$ on $y$ was experimentally determined by Chow et al. [17] in the temperature range of $T =$ 523–973 K. Their results of $T = 823$ and 973 K are shown as open squares and circles, respectively, in Fig. 3. In this figure, the ordinate and the abscissa indicate $D$ and $y$, respectively. According to their results [17], $D$ is rather insensitive to $y$ at temperatures around $T = 900$ K. Thus, we may expect that $D$ is close to the tracer diffusion coefficient $D^{Cu}_{Pd}$ of Pd in Cu and independent of $y$ [24, 25]. The temperature dependence of $D^{Cu}_{Pd}$ is described by the equation

$$D^{Cu}_{Pd} = D^{Cu}_{Pd_0} \exp\left(-\frac{Q}{RT}\right), \quad (2)$$

where $D^{Cu}_{Pd_0}$ and $Q$ are the pre-exponential factor and the activation enthalpy, respectively. The following values are reported for $D^{Cu}_{Pd}$ : $D^{Cu}_{Pd_0} = 1.71 \times 10^{-4}\,m^2/s$ and $Q =$ 228 kJ/mol [26]. Using these parameters, $D^{Cu}_{Pd}$ was calculated from Eq. 2. The calculations of $T = 823$ and 973 K are shown as horizontal solid lines in Fig. 3. As can be seen, $D$ is three orders of magnitude larger for the open squares than for the solid line at $T = 823$ K and more than one order of magnitude larger for the open circles than for the solid line at $T = 973$ K. This implies that the contribution of boundary diffusion is included in the values of $D$ shown with the open symbols. Actually, in the diffusion experiment, fine-grained polycrystalline Cu/Pd diffusion couples were used by Chow et al. [17]. The temperature dependence of the boundary diffusion

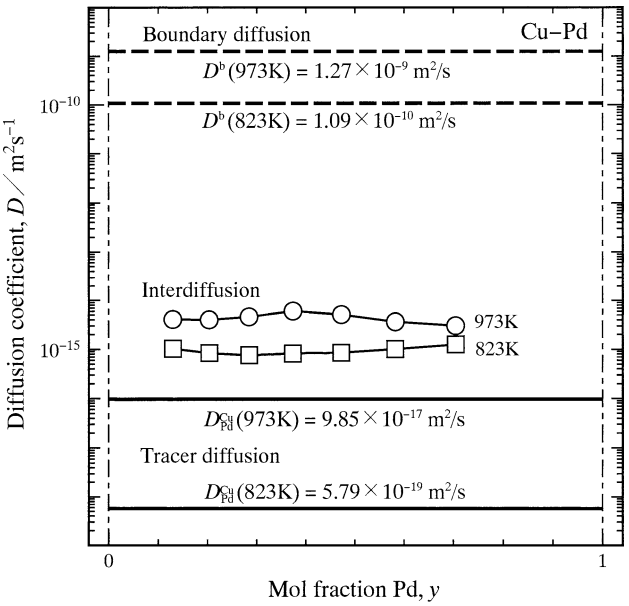


**Fig. 3** The diffusion coefficient $D$ versus the mole fraction $y$ of Pd. The results of the interdiffusion coefficient in the fcc phase of the binary Cu–Pd system at $T = 823$ and 973 K reported by Chow et al. [17] are shown as *open squares* and *circles*, respectively. *Solid lines* indicate the corresponding results of the tracer diffusion coefficient $D^{Cu}_{Pd}$ of Pd in Cu [26], and *dashed lines* show those of the boundary diffusion coefficient $D^b$ of Ag in Cu [28]

coefficient $D^b$ of Pd in the grain boundary of Cu is described by the following equation of the same formula as Eq. 2.

$$\sigma\delta D^b = \sigma\delta D^b_0 \exp\left(-\frac{Q^b}{RT}\right) \quad (3)$$

Here, $\delta$ and $\sigma$ are the thickness and the segregation factor, respectively, of the grain boundary. The dependence of $\sigma\delta D^b$ on $T$ was experimentally determined by many researchers [18, 20]. Although $\sigma\delta D^b$ should be independent of $t$, Chakraborty et al. [20] reported that $\sigma\delta D^b$ monotonically decreased with increasing annealing time $t$. Like Chow et al. [17], Chakraborty et al. [20] used fine-grained polycrystalline Cu/Pd diffusion couples for the experiment. In such diffusion couples, grain growth occurs during annealing, and hence the contribution of boundary diffusion to interdiffusion gradually decreases with increasing annealing time $t$. Thus, the monotonically decreasing dependence of $\sigma\delta D^b$ on $t$ is attributed to the grain growth in the diffusion couple. The values of $\sigma\delta D^b$ determined by Bukaluk [18] are close to those reported by Chakraborty et al. [20]. This implies that the influence of the grain growth is included also in the result by Bukaluk [18]. In contrast, the dependence of $\sigma\delta D^b$ on $T$ for the boundary diffusion of Ag in Cu was experimentally determined by Renouf [27]. On the basis of his result, the following parameters were revaluated by Kaur et al. [28]:

$\sigma\delta D_0^{\mathrm{b}} = 9.39 \times 10^{-13}$ m$^3$/s and $Q^{\mathrm{b}} = 109.3$ kJ/mol. Using these parameters and assuming $\delta = 1$ nm and $\sigma = 1$, $D^{\mathrm{b}}$ was calculated from Eq. 3. The calculations of $T = 823$ and 973 K are shown as horizontal dashed lines in Fig. 3. Since the atomic number $Z_{\mathrm{Ag}} = 47$ of Ag is slightly greater than that $Z_{\mathrm{Pd}} = 46$ of Pd, $\sigma\delta D^{\mathrm{b}}$ may be lightly smaller for Ag in Cu than for Pd in Cu. Therefore, the dashed lines in Fig. 3 will provide lower limits of $\sigma\delta D^{\mathrm{b}}$ for Pd in Cu. As can be seen, the open symbols give intermediate values of $D$ smaller than $\sigma\delta D^{\mathrm{b}}$ but greater than $D_{\mathrm{Pd}}^{\mathrm{Cu}}$. This means that boundary diffusion as well as volume diffusion contributes to the intermediate values of $D$. Hence, the horizontal solid lines rather than the open symbols can give more reliable information on $D$. Assuming $D = D_{\mathrm{Pd}}^{\mathrm{Cu}}$, the concentration profile of Pd in the Cu by volume diffusion was calculated from Eq. 1. The calculation with $T = 1{,}023$ K and $t = 70.02$ h (252.1 ks) is shown as the dashed curve in Fig. 2a. As can be seen, the thickness of the DIR region is more than twice greater than the penetration depth of the volume diffusion. Consequently, alloying of Cu with Pd occurs fast due to DIR under the present annealing conditions. The penetration depth by volume diffusion is about 25 μm for Pd into Cu and Cu into Pd as shown with the dashed curve and the open circles, respectively, in Fig. 2a. This also guarantees that $D$ is insensitive to $y$.

According to the concentration profile in Fig. 2, the concentration of Pd in the DIR region monotonically decreases from $y = 0.495$ to $y = 0.010$ with increasing distance $x$ from the Pd boundary to the Cu boundary. Since the Pd boundary is rather stationary and volume diffusion is sluggish in the DIR region, the maximum value $y = 0.495$ may correspond to the initial composition $y_{\mathrm{i}}$ of the DIR region formed at the beginning of the reaction. The experimental values of $y_{\mathrm{i}}$ are plotted as open circles with error bars against the annealing temperature $T$ in Fig. 4. As can be seen, $y_{\mathrm{i}}$ is close to or smaller than 0.5.

## Growth behavior of DIR region

As mentioned above, the DIR region grows rather predominantly toward the Cu but slightly into the Pd at $T = 923$–$1{,}023$ K. From the DICOM photographs like Fig. 1, the mean thickness $l$ of the DIR region was determined by the equation [11]

$$l = \frac{A}{w}, \tag{4}$$

where $A$ and $w$ are the total area and the total length of the DIR region, respectively, on the cross-section. As previously mentioned, however, the number of visible voids ahead of the Cu boundary is larger for Etching B than for Etching A. Such voids obstruct the identification of the Cu boundary. Thus, the DICOM photograph with Etching

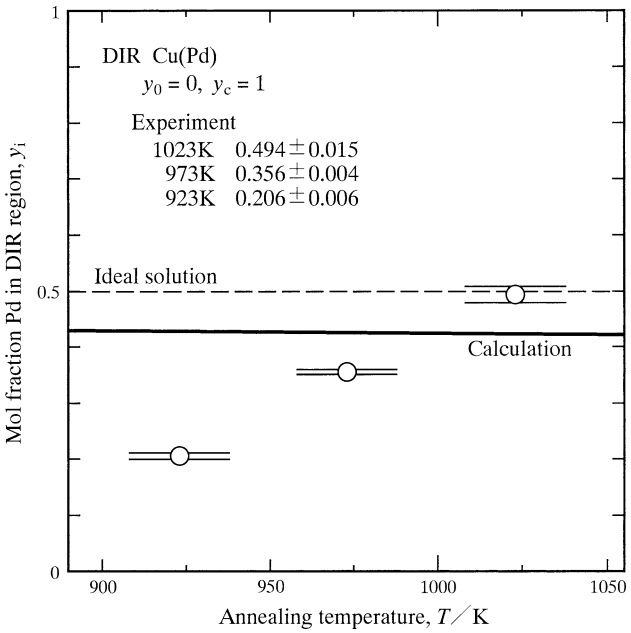


**Fig. 4** The mole fraction $y_{\mathrm{i}}$ of Pd in the DIR region at the Pd boundary versus the annealing temperature $T$ shown as *open circles* with error bars. The calculation with Eqs. 8–11 is indicated as a *solid curve*

A was used to measure the area $A$ and the length $w$. The result is indicated in Fig. 5. In this figure, the ordinate and the abscissa show the logarithms of $l$ and $t$, respectively, and open rhombuses, squares, and circles indicate the results of $T = 923$, 973, and 1,023 K, respectively. As can be seen, the thickness $l$ monotonically increases with increasing annealing time $t$ at all the annealing temperatures. The higher the annealing temperature is, the faster the DIR region grows. Furthermore, the plotted points are located on parallel straight lines. This means that $l$ is mathematically described as a power function of $t$ by the equation

$$l = k\left(\frac{t}{t_0}\right)^n. \tag{5}$$

Here, $t_0$ is unit time, 1 s. It is adopted to make the argument $t/t_0$ of the power function dimensionless. The proportionality coefficient $k$ has the same dimension as the thickness $l$, but the exponent $n$ is dimensionless. Considering an equivalent value of $n$ at all the annealing temperatures, $k$ and $n$ were simultaneously evaluated from the plotted points in Fig. 5 by the least-squares method. The evaluated values are indicated in Fig. 5. Using these values, $l$ was calculated as a function of $t$ from Eq. 5. The calculations of $T = 923$, 973, and 1,023 K are shown as dotted, dashed, and solid lines, respectively, in Fig. 5. As can be seen, $n$ is rather close to 1/4 significantly smaller than 1/2. Thus, the growth of the DIR region is surely controlled by boundary diffusion [29]. On the other hand,

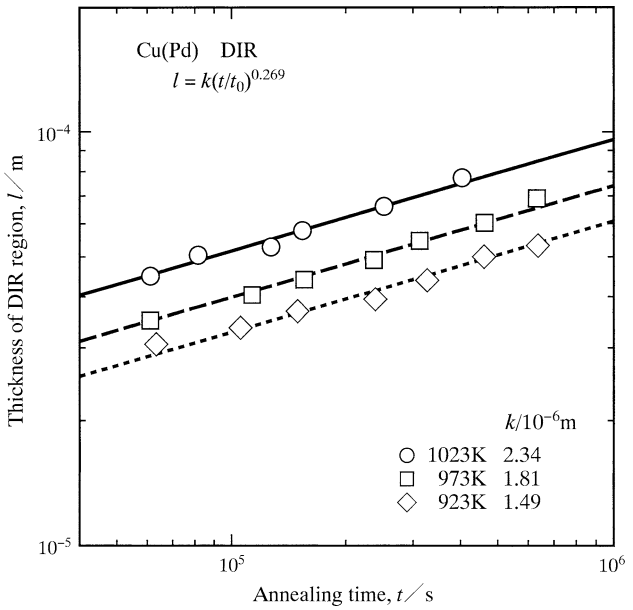


**Fig. 5** The thickness $l$ of the DIR region versus the annealing time $t$ shown as *open rhombuses*, *squares*, and *circles* at $T = 923$, 973, and 1,023 K, respectively. The calculations with Eq. 5 for $T = 923$, 973, and 1,023 K are indicated as *dotted*, *dashed*, and *solid lines*, respectively

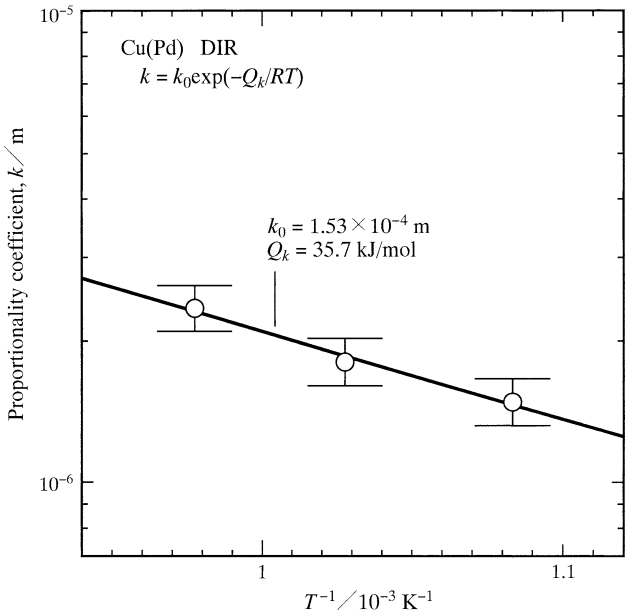


**Fig. 6** The proportionality coefficient $k$ versus the reciprocal of the annealing temperature $T$ shown as *open circles* with error bars. A *solid line* indicates the calculation with Eq. 6

the values of $k$ are plotted as open circles with error bars against $T$ in Fig. 6. In this figure, the ordinate shows the logarithm of $k$, and the abscissa indicates the reciprocal of $T$. As can be seen, the open circles lie well on a straight line. Therefore, the dependence of $k$ on $T$ is expressed by the following equation of the same formula as Eqs. 2 and 3.

$$k = k_0 \exp\left(-\frac{Q_k}{RT}\right) \tag{6}$$

The pre-exponential factor $k_0$ and the activation enthalpy $Q_k$ in Eq. 6 were evaluated from the open circles by the least-squares method as shown with a solid line in Fig. 6. The evaluation provides $k_0 = 1.53 \times 10^{-4}$ m and $Q_k = 35.7$ kJ/mol. The rate-controlling process may be estimated from the value of $Q_k$. However, the dimension of $k$ is m, but that of $D$ or $D^{\mathrm{b}}$ is m$^2$/s. Hence, $Q_k = 35.7$ kJ/mol cannot be directly compared with $Q = 228$ kJ/mol or $Q^{\mathrm{b}} = 109.3$ kJ/mol. The rate-controlling process will be estimated using a kinetic model later on.

## Discussion

### Chemical composition

Fine grains formed by DIR in the A(B) system are schematically drawn in Fig. 7. Here, the notation A(B) indicates that a solute B diffuses into either a pure metal A or a binary A–B alloy of the A-rich single-phase according to convention. In a previous study [21], a chemical driving force (CDF) model was proposed to evaluate the composition of the DIR region in the A(B) system. Furthermore, like Cu and Pd, elements A and B are nonvolatile at annealing temperatures. If the DIR region with composition $y_{\mathrm{i}}$ is formed in the untransformed matrix with composition $y_0$ from the source alloy with composition $y_{\mathrm{c}}$, the CDF $\Delta G_{\mathrm{m}}$ is mathematically described as a function of $y_{\mathrm{i}}$ by the following equation according to the CDF model [21]:

$$\Delta G_{\mathrm{m}}(y_{\mathrm{i}}) = \frac{1}{y_{\mathrm{c}} - y_0}\{(y_{\mathrm{i}} - y_0)G_{\mathrm{m}}(y_{\mathrm{c}}) + (y_{\mathrm{c}} - y_{\mathrm{i}})G_{\mathrm{m}}(y_0)\} - G_{\mathrm{m}}(y_{\mathrm{i}}) \tag{7}$$

Here, $G_{\mathrm{m}}$ is the molar Gibbs energy of the primary solid-solution ($\alpha$) phase of element A, and $G_{\mathrm{m}}(y_{\mathrm{c}})$, $G_{\mathrm{m}}(y_0)$, and $G_{\mathrm{m}}(y_{\mathrm{i}})$ are the values of $G_{\mathrm{m}}$ at $y = y_{\mathrm{c}}$, $y_0$, and $y_{\mathrm{i}}$, respectively. When the formation of the DIR region occurs spontaneously, $\Delta G_{\mathrm{m}}$ takes a positive value. For the maximum value of $\Delta G_{\mathrm{m}}$, the following relationship holds among $y_{\mathrm{c}}$, $y_0$, and $y_{\mathrm{i}}$ [21]:

$$G_{\mathrm{m}}(y_{\mathrm{c}}) - G_{\mathrm{m}}(y_0) + (y_{\mathrm{c}} - y_0)\{G_{\mathrm{A}}(y_{\mathrm{i}}) - G_{\mathrm{B}}(y_{\mathrm{i}})\} = 0, \tag{8}$$

where $G_{\mathrm{A}}$ and $G_{\mathrm{B}}$ are the partial molar Gibbs energies of elements A and B, respectively, in the $\alpha$ phase. Furthermore, $y_0 < y_{\mathrm{i}}$, $y_{\mathrm{i}} < y_{\mathrm{c}}$, and $y_{\mathrm{c}} < y_{\mathrm{s}}$, where $y_{\mathrm{s}}$ is the solubility of element B in the $\alpha$ phase. The molar Gibbs energy $G_{\mathrm{m}}$ is expressed as a function of the mole fraction $y$ of element B by the equation

$$G_m = (1-y)^{\circ}G_A + y^{\circ}G_B + RT\{(1-y)\ln(1-y) + y\ln y\} + {}^{E}G_m. \quad (9)$$

Here, $^{\circ}G_A$ is the value of $G_A$ at $y = 0$, $^{\circ}G_B$ is that of $G_B$ at $y = 1$, $^{E}G_m$ is an excess Gibbs energy, and $R$ is the gas constant. According to a subregular solution model [30], $^{E}G_m$ is described as

$$^{E}G_m = y(1-y)\{{}^{0}L + {}^{1}L(1-2y) + {}^{2}L(1-2y)^2\}, \quad (10)$$

where $^{j}L$ ($j = 0, 1, 2$) is a thermodynamic interaction parameter between elements A and B in the $\alpha$ phase. From Eqs. 9 and 10 we obtain

$$G_A = {}^{\circ}G_A + RT\ln(1-y) + y^2\{{}^{0}L + {}^{1}L(1-2y) + {}^{2}L(1-2y)^2\} + 2(1-y)y^2\{{}^{1}L + {}^{2}L2(1-2y)\} \quad (11a)$$

and

$$G_B = {}^{\circ}G_B + RT\ln y + (1-y)^2\{{}^{0}L + {}^{1}L(1-2y) + {}^{2}L(1-2y)^2\} - 2(1-y)^2y\{{}^{1}L + {}^{2}L2(1-2y)\} \quad (11b)$$

Inserting Eqs. 9–11 into Eq. 8, $y_i$ is calculated as a function of $T$ for given values of $y_0$ and $y_c$. As to DIR in the Cu(Pd) system, the calculation was carried out using the following parameters: $y_0 = 0$ and $y_c = 1$; and $^{0}L = -44505 + 15.478T$, $^{1}L = -4477 - 10.28T$ and $^{2}L = 0$ J/mol [31]. The result is shown as the solid curve in Fig. 4. If the DIR region is a thermodynamically ideal solution, $y_i$ is equal to 0.5 for $y_0 = 0$ and $y_c = 1$ as indicated as the horizontal dashed line in Fig. 4 [21]. According to the solid curve, however, $y_i$ is smaller than 0.5 at $T = 923$–1,023 K. Nevertheless, $y_i$ gradually increases with decreasing annealing temperature $T$ and thus approaches 0.5 at low temperatures. Such temperature dependence of $y_i$ is attributed to the thermodynamic interaction between Cu and Pd in the fcc phase. On the other hand, the open circles in Fig. 4 show the experimental values of $y_i$ as mentioned earlier. As can be seen, $y_i$ is rather close to each other between the open circles and the solid curve at $T = 973$–1,023 K, but much smaller for the open circle than for the solid curve at $T = 923$ K. Furthermore, at $T = 1{,}023$ K, the open circle is more close to the dashed line than to the solid line.

As previously mentioned, the CDF $\Delta G_m$ for the formation of DIR region is given by Eq. 7. From this equation, the dependence of $\Delta G_m$ on $y_i$ was calculated for $y_0 = 0$ and $y_c = 1$. The results of $T = 923$, 973, and 1,023 K are shown as solid curves in Fig. 8a–c, respectively. In this figure, the ordinate and the abscissa indicate $\Delta G_m$ and $y_i$, respectively, and $y_i^e$ and $y_i^c$ stand for the experimental and calculated values of $y_i$, respectively. The solid curves in Fig. 8 provide the following values: $\Delta G_m(y_i^e) = 10.2$ kJ/mol and $\Delta G_m(y_i^c) = 13.1$ kJ/mol at $T = 923$ K; $\Delta G_m(y_i^e) = 13.0$ kJ/mol and $\Delta G_m(y_i^c) = 13.2$ kJ/mol at $T = 973$ K; and $\Delta G_m(y_i^e) = 13.1$ kJ/mol and $\Delta G_m(y_i^c) = 13.4$ kJ/mol at $T = 1{,}023$ K. If the ratio $h$ is defined as

$$h \equiv \frac{\Delta G_m(y_i^e)}{\Delta G_m(y_i^c)}, \quad (12)$$

we obtain $h = 0.756$, 0.980, and 0.981 at $T = 923$, 973, and 1,023 K, respectively. Thus, at $T = 973$–1,023 K, $\Delta G_m(y_i^e)$ is very close to $\Delta G_m(y_i^c)$, though $y_i^e$ slightly deviates from $y_i^c$. Consequently, it is concluded that the thermodynamic behavior of DIR in the Cu(Pd) system is adequately described by the CDF model at $T = 973$–1,023 K. On the other hand, at $T = 923$ K, $\Delta G_m(y_i^e)$ is smaller by 24% than $\Delta G_m(y_i^c)$. The CDF model implicitly assumes that the rate of supply of atoms to the DIR region is close to each other between elements A and B. However, in the Cu(Pd) system, the formation of the DIR region may be realized mainly by the supply of Pd atoms into the Cu. As the annealing temperature decreases, the supply rate monotonically decreases, and thus shortage of the supply becomes considerable. This may be the reason why $y_i^e$ is much smaller than $y_i^c$ at $T = 923$ K.

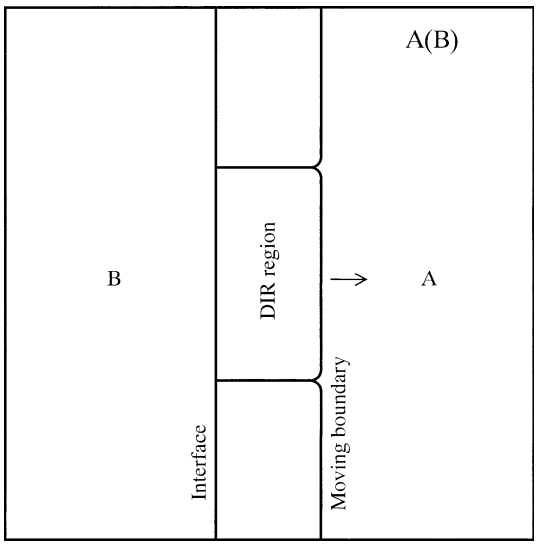


**Fig. 7** Schematic drawing of fine grains in the DIR region for the A(B) system

DIR in various binary alloy systems similar to the Cu–Pd system has been experimentally studied by many investigators [32–35]. For instance, Hartung and Schmitz [32] observed DIR in the Au–Cu system using Au/Cu diffusion couples at $T = 703$ K. According to their observation, the DIR regions are formed on both sides of the Au/Cu interface in the diffusion couple. This means that DIR in the Au(Cu) and Cu(Au) systems

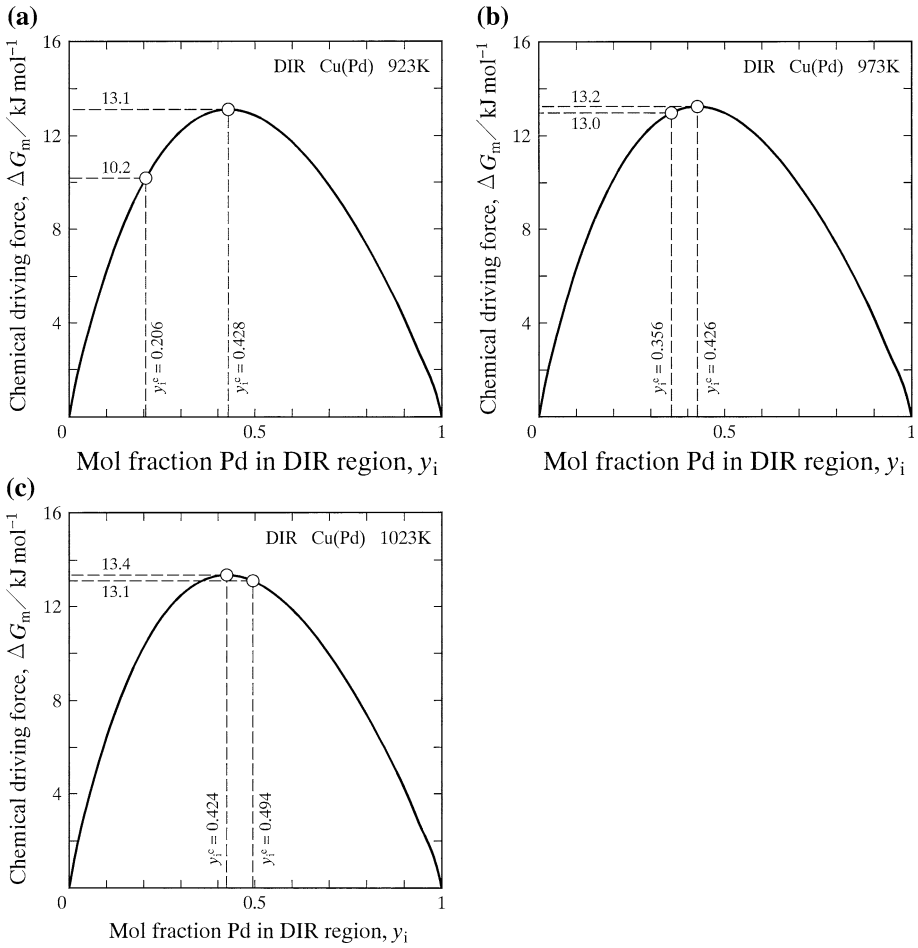


**Fig. 8** The chemical driving force $\Delta G_m$ as a function of the composition $y_i$ for $y_0 = 0$ and $y_c = 1$ at **a** $T = 923$ K, **b** $T = 973$ K, and **c** $T = 1{,}023$ K. The experimental value of $y_i$ is shown as $y_i^e$, and the value of $y_i$ calculated from Eqs. 8–11 is denoted by $y_i^c$

simultaneously occurs under their annealing conditions. The mole fraction of Cu in the DIR region corresponding to $y_i$ is 0.17 and 0.81 for the Au(Cu) and Cu(Au) systems, respectively. The CDF model is only applicable to DIR in a single A(B) system. Thus, duplicated values of $y_i$ for DIR in double A(B) and B(A) systems cannot be treated in a straightforward manner by the CDF model.

## Kinetics

In order to estimate the rate of supply of solute atoms to the moving boundary of the DIR region, Li and Hillert [36] assumed that the shape of each fine grain in the DIR region is columnar and the diffusion coefficient along the moving boundary is much greater than that along the circular boundary of the columnar fine grain. Hence, they obtained the following equation to express the rate of supply of the solute along the circular boundary to the moving boundary:

$$\frac{\mathrm{d}m}{\mathrm{d}t} = -\frac{1}{2}\pi s\delta\frac{D^{\mathrm{b}}\mathrm{d}y}{V_{\mathrm{m}}\mathrm{d}x} = \frac{\pi s\delta}{2}\frac{D^{\mathrm{b}}}{V_{\mathrm{m}}}\frac{y_{\mathrm{i}} - y_{\mathrm{e}}}{l}, \tag{13}$$

where $m$ is the amount of the solute supplied to the moving boundary, $s$ is the diameter of the columnar grain, $V_{\mathrm{m}}$ is the molar volume of the columnar grain, and $y_{\mathrm{e}}$ is the mole fraction of the solute in the columnar grain at the moving boundary. Here, $m$, $s$, and $V_{\mathrm{m}}$ are measured in mol, m, and m$^3$/mol, respectively. For such geometry, the supply rate d$m$/d$t$ is correlated with the migration rate $r$ of the moving boundary by the equation

$$\frac{\mathrm{d}m}{\mathrm{d}t} = \pi\left(\frac{s}{2}\right)^2\frac{2y_{\mathrm{e}} - y_0}{V_{\mathrm{m}}}r. \tag{14}$$

On the other hand, the migration rate $r$ is related to the effective driving force $\Delta^{\mathrm{ef}}G$ acting on the moving boundary by the equation

$$r = \frac{\mathrm{d}l}{\mathrm{d}t} = M\Delta^{\mathrm{ef}}G, \tag{15}$$

where $M$ is the mobility of the moving boundary. Equation 15 shows that the growth rate d$l$/d$t$ of the DIR region is equal to $r$ and $r$ is proportional to $\Delta^{\mathrm{ef}}G$. Since $\Delta^{\mathrm{ef}}G$ possesses the dimension of force per unit area or energy per unit volume, the dimension of $M$ is m$^4$/Js on condition that $l$, $t$, and $\Delta^{\mathrm{ef}}G$ are measured in m, s, and J/m$^3$, respectively. In order to estimate the effective driving force $\Delta^{\mathrm{ef}}G$, an energy balance (EB) model was suggested in a

previous study [37]. Combining the geometrical assumption by Li and Hillert with the EB model, a new extended (NE) model was proposed to describe mathematically the growth rate of the DIR region in the A(B) system in a previous study [22]. When one mole of the DIR region with composition $y_e$ is produced from $(y_e - y_0)/(1 - y_0)$ mole of element B and $(1 - y_e)/(1 - y_0)$ mole of the $\alpha$ phase with composition $y_0$, a penetration zone of element B will be formed by volume diffusion in the untransformed matrix of the $\alpha$ phase ahead of the moving boundary of the DIR region. Under such conditions, $\Delta^{ef}G$ is expressed by the following equation according to the NE model [22]:

$$\Delta^{ef}G = (1 - y_e)\left\{\frac{RT}{V_m}\left(\ln\frac{1 - y_{nf}}{1 - y_e} + \frac{y_0}{1 - y_0}\ln\frac{y_{nf}}{y_e}\right) - Y\eta^2\frac{(y_{nf} - y_0)^2}{1 - y_0}\right\}. \quad (16)$$

Here, $y_{nf}$ is the composition of the penetration zone at the interatomic distance $\lambda$ from the moving boundary, $Y$ is the biaxial elastic modulus of the untransformed matrix along the plane parallel to the moving boundary, and $\eta$ is the misfit parameter. If the $\alpha$ phase is elastically isotropic, $Y$ is described as

$$Y = \frac{E}{1 - \nu}, \quad (17)$$

where $E$ and $\nu$ are the Young's modulus and the Poisson's ratio, respectively. Let $y_{pf}$ be the composition in the penetration zone at the interface between the untransformed matrix and the moving boundary. This interface is called the front interface. The composition $y_{nf}$ in Eq. 16 is approximately expressed as a function of $y_{pf}$, $y_0$, $r$, and $\lambda$ by the equation [22]

$$y_{nf} = y_0 + (y_{pf} - y_0)\exp(-r\lambda/D), \quad (18)$$

where $D$ is the diffusion coefficient for volume diffusion of element B in the penetration zone. Considering the local equilibrium between the moving boundary and the penetration zone at the front interface, $y_{pf}$ is evaluated by the parallel-tangent construction (PTC) method [38]. When the concentration gradient of element B across the moving boundary is negligible, the following equation is obtained by the PTC method:

$$\ln\frac{y_{pf}}{1 - y_{pf}} + \frac{2YV_m\eta^2}{RT}(y_{pf} - y_0) = \ln\frac{y_e}{1 - y_e}. \quad (19)$$

In this equation, $y_e$ is a function of $l$, $s$, $r$, $\delta$, and $D^b$ for a given value of $y_i$ as follows:

$$y_e = \frac{y_0 slr + y_i 2\delta D^b}{slr + 2\delta D^b}. \quad (20)$$

Equation 20 is obtained by elimination of the term d$m$/d$t$ from Eqs. 13 and 14. As to the parameters in Eqs. 16–18, the following values were reported for the Cu(Pd) system: $E = 129.8$ GPa and $\nu = 0.343$ [39]; $V_m = 7.1106 \times 10^{-6}$ m$^3$/mol and $\eta = 0.076355$ [26]; and $\lambda = 0.3$ nm [22]. Using these parameters, the relationship between $l$ and $t$ is evaluated from Eqs. 15–20. The evaluation will be explained below.

Adopting $y_0 = 0$ and $D = D_{Pd}^{Cu}$, the thickness $l_i$ was numerically calculated at each experimental annealing time $t_i$ from Eqs. 15–20. As mentioned earlier, however, no reliable information is available for $\sigma\delta D^b$ of Pd in Cu. Thus, the parameters $\sigma\delta D_0^b = 9.39 \times 10^{-13}$ m$^3$/s and $Q^b = 109.3$ kJ/mol reported by Kaur et al. [28] for $\sigma\delta D^b$ of Ag in Cu were used to estimate $\sigma\delta D^b$ of Pd in Cu from Eq. 3. In the case of the complete solid-solution phase, $\sigma$ may not be so different from unity. Since there is no dependable value of $\sigma$ for the fcc phase in the binary Cu–Pd system, the value $\sigma = 1$ was adopted for simplicity. For the calculation of $l_i$, the value of $y_i$ shown as the solid curve in Fig. 4 was utilized, and $s$ was assumed to be equal to $l$. As a result, the mobility $M$ in Eq. 15 remains as the only unknown parameter. Unfortunately, however, no trustable information on $M$ is obtainable for DIR in the Cu(Pd) system. Thus, $M$ was selected as the fitting parameter to minimize the function $f$ defined as

$$f = \sum_{i=1}^{p}\left(l_i - l_i^e\right)^2. \quad (21)$$

Here, $l_i^e$ is the experimental value of $l$ at $t = t_i$, and $p = 7$ and 6 at $T = 923$–973 and 1,023 K, respectively. From the open symbols in Fig. 5, $M = 1.64 \times 10^{-18}$, $2.03 \times 10^{-18}$, and $3.81 \times 10^{-18}$ m$^4$/J s are obtained at $T = 923$, 973, and 1,023 K, respectively. Using these values of $M$, $l$ was calculated as a function of $t$ from Eqs. 15–20. The calculations of $T = 923$, 973, and 1,023 K are shown as solid curves in Fig. 9a–c, respectively. In this figure, like Fig. 5, the ordinate and the abscissa indicate the logarithms of $l$ and $t$, respectively. On the other hand, the experimental points of $T = 923$, 973, and 1,023 K in Fig. 5 are plotted again as open circles in Fig. 9a–c, respectively. At first glance, however, the plotted points at the shorter annealing times seem to deviate rather remarkably from the corresponding solid curve. As mentioned earlier, the minimization for the summation of the differences between $l_i$ and $l_i^e$ was carried out using the function $f$ defined by Eq. 21. In contrast, in Fig. 9, the ordinate indicates the logarithm of $l$. Therefore, the deviation from the corresponding curve is visually exaggerated for smaller values of $l$ at the shorter annealing times in Fig. 9. As shown with extrapolated dashed lines in Fig. 9, each solid curve is almost straight at $t < 10^5$ s and $t > 5 \times 10^7$ s. Hence, in these annealing time ranges, $l$ is described as a power function of $t$ by Eq. 5. If the growth of the DIR

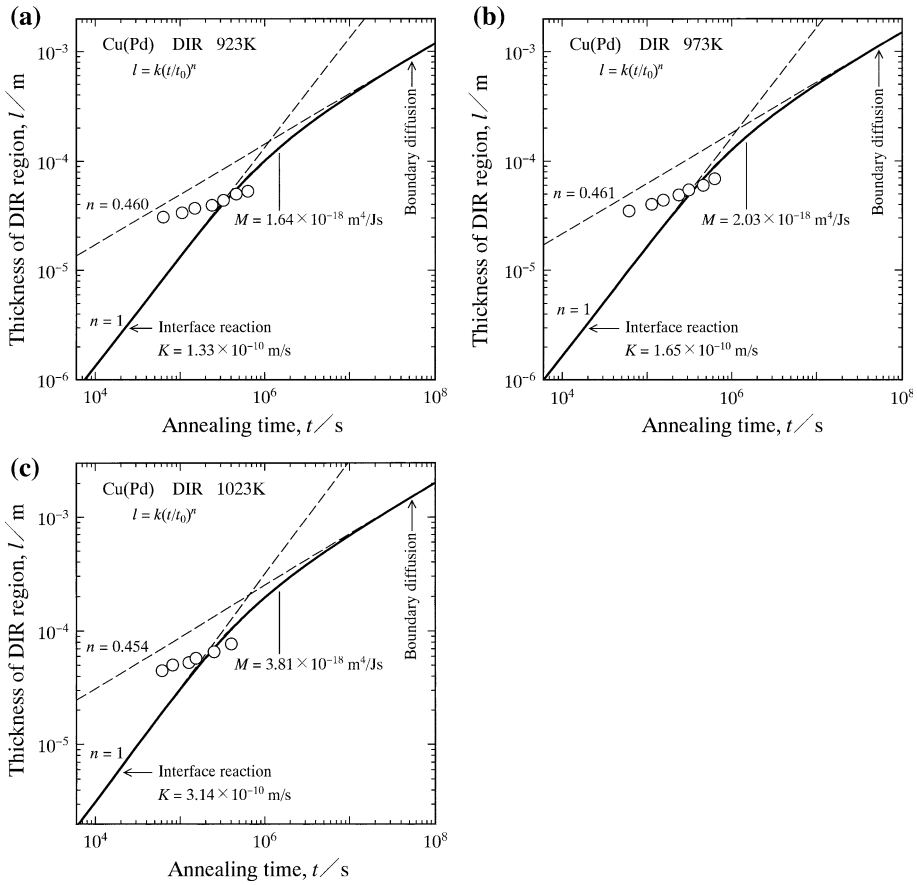


**Fig. 9** The experimental results in Fig. 5 are represented as *open circles*: **a** $T = 923$ K, **b** $T = 973$ K, and **c** $T = 1{,}023$ K. *Solid curves* indicate the calculations with Eqs. 15–20, and *dashed lines* show the extrapolations of the *solid curves* in the early and late stages of the reaction

region is controlled by the interface reaction at the moving boundary, $l$ is proportional to $t$ and thus $n$ is equal to unity [22, 36]. This is just the case at $t < 10^5$ s. Inserting $n = 1$ into Eq. 5, we obtain the following equation for this type of rate-controlling process:

$$l = \frac{k}{t_0} t = Kt. \tag{22}$$

Here, $K$ is the kinetic coefficient with a dimension of m/s. From the straight part of the solid curve at $t < 10^5$ s in Fig. 9, $K = 1.33 \times 10^{-10}$, $1.65 \times 10^{-10}$, and $3.14 \times 10^{-10}$ m/s are obtained at $T = 923$, 973, and 1,023 K, respectively. On the other hand, $n = 0.460$, 0.461, and 0.454 are evaluated at $T = 923$, 973, and 1,023 K, respectively, for the straight part of the solid curve at $t > 5 \times 10^7$ s in Fig. 9. Consequently, $n$ gradually decreases from unity to the minimum value smaller than 1/2 with increasing annealing time at $10^5$ s $< t < 5 \times 10^7$ s. In the early stages, $l$ is very small, and hence an abundant amount of the solute can be transported by the boundary diffusion across the DIR region. In such a case, the interface reaction at the moving boundary becomes the bottleneck for the growth of the DIR region. On the other hand, in the late stages, $l$ is very large, and thus the solute has to be transported by the boundary diffusion over long distances across the DIR region. As a result, the boundary diffusion governs the rate-controlling process, but the interface reaction is no longer the bottleneck. Therefore, the growth of the DIR region is controlled by the interface reaction in the early stages but by the boundary diffusion in the late stages [22, 36]. Although the numerical calculation satisfactorily re-creates the absolute value of $l$, the solid curves in Fig. 9 cannot necessarily reproduce $n \cong 1/4$ even in the late stages. The value $n = 1/4$ implies that $s$ increases in proportion to the square root of $t$ [29]. Such dependence of $s$ on $t$ is called the parabolic relationship. On the other hand, in the numerical calculation, it is assumed that $s = l$. In order to test the validity of this assumption, the metallographical observation of the DIR region is necessary. As shown in Fig. 1b, the polycrystalline microstructure of the DIR region was recognized on the DICOM photograph with Etching B. However, the DIR region alloyed with Pd is rather corrosion resistant. Hence, each polycrystalline grain cannot be so clearly distinguished even on this type of DICOM photograph. Consequently, the grain growth of the DIR region could not be accurately detected in a metallographical manner. Furthermore, there is no reliable information on $\sigma\delta D^b$ of Pd in

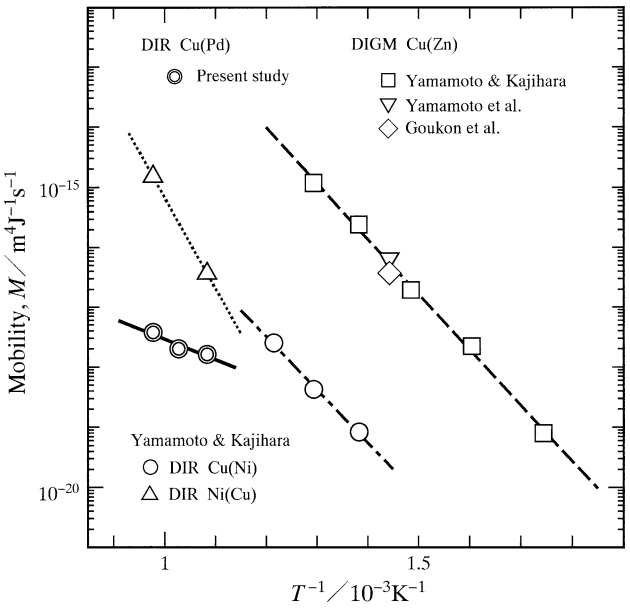


**Fig. 10** The mobility $M$ for the moving boundary of the DIR region versus the reciprocal of the annealing temperature $T$ shown as *open double circles*. A *solid line* indicates the calculation with Eq. 23. *Open circles* and *triangles* indicate the corresponding results of DIR in the Cu(Ni) [14] and Ni(Cu) [22] systems, respectively, and different *open symbols* show those of DIGM in the Cu(Zn) system [40–42]

Cu. Thus, the corresponding value of Ag in Cu was used in the present study. If $s$ is empirically expressed as a function of $t$ and trustable information becomes available for $\sigma\delta D^{b}$, the value $n \cong 1/4$ may be reproduced by the numerical calculation.

As stated above, $M$ was chosen as the fitting parameter to calculate the model curves in Fig. 9. The values of $M$ are plotted as open double circles against $T$ in Fig. 10. In this figure, the ordinate shows the logarithm of $M$, and the abscissa indicates the reciprocal of $T$. Although the open double circles are slightly scattered, the dependence of $M$ on $T$ may be expressed by the following equation of the same formula as Eqs. 2, 3, and 6:

$$M = M_0 \exp\left(-\frac{Q_M}{RT}\right). \tag{23}$$

From the open double circles in Fig. 10, the pre-exponential factor and the activation enthalpy in Eq. 23 were estimated to be $M_0 = 7.94 \times 10^{-15}$ m$^4$/J s and $Q_M =$ 65.7 kJ/mol, respectively, by the least-squares method as shown with a solid line. On the other hand, the values of $M$ for DIR in the Cu(Ni) system reported in a previous study [14] are shown as open circles with a dashed and dotted line of $M_0 = 1.15 \times 10^{-7}$ m$^4$/J s and $Q_M =$ 168 kJ/mol in Fig. 10. Furthermore, in this figure, the corresponding result for DIR in the Ni(Cu) system [22] is indicated as open triangles with a dotted line of $M_0 =$ 1.03 m$^4$/J s and $Q_M = 290$ kJ/mol, and those for DIGM in the Cu(Zn) system [40–42] are shown as different open symbols with a dashed line of $M_0 = 1.24 \times 10^{-3}$ m$^4$/J s and $Q_M = 177$ kJ/mol. Extrapolating the solid line to the lower temperature range of $T = 723$–$823$ K ($T^{-1} = 1.22 \times 10^{-3}$–$1.38 \times 10^{-3}$ K$^{-1}$), we may find that $M$ is close to each other between the Cu(Pd) and Cu(Ni) systems. On the other hand, at $T = 923$–$1{,}023$ K ($T^{-1} = 9.78 \times 10^{-4}$–$1.08 \times 10^{-3}$ K$^{-1}$), the solid line is located on the lower side of the dashed and dotted line, and thus $M$ is smaller for the Cu(Pd) system than for the Cu(Ni) system. Since no dependable information is obtainable for $\sigma\delta D^{b}$ of Pd in Cu, $\sigma\delta D^{b}$ of Ag in Cu was used for the calculation of $M$ in Fig. 10 as mentioned earlier. For meaningful comparison of $M$ between the Cu(Pd) and Cu(Ni) systems, reliable information on $\sigma\delta D^{b}$ of Pd in Cu is essentially important.

## Conclusions

The kinetics of DIR in the Cu(Pd) system was experimentally examined using the Cu/Pd/Cu diffusion couple in the temperature range between $T = 923$ and 1,023 K. During annealing, the DIR region alloyed with Pd rather predominantly grows into the Cu from the Cu/Pd interface. The concentration of Pd on the Pd-rich side in the DIR region is independent of the annealing time but increases with increasing annealing temperature. The CDF model proposed in a previous study [21] quantitatively explains the results of $T = 973$–$1{,}023$ K but not that of $T = 923$ K. The thickness $l$ of the DIR region monotonically increases with increasing annealing time $t$. The higher the annealing temperature is, the faster the DIR region grows. The growth rate of the DIR region was numerically calculated using the NE model proposed in a previous study [22]. The overall growth rate of the DIR region is satisfactorily reproduced by the numerical calculation.

**Acknowledgements** The present study was supported by the Iketani Science and Technology Foundation in Japan. The study was also partially supported by a Grant-in-Aid for Scientific Research from the Ministry of Education, Culture, Sports, Science, and Technology of Japan.

## References

1. den Broeder FJA (1985) Thin Solid Films 124:135
2. Shewmon PG, Meyrick G (1985) Metals/materials technology series 8408-018. Am Soc Metals, Metals Park, p 1
3. Handwerker CA (1987) In: Gupta D (ed) Diffusion phenomena in thin films, Noyes, New Jersey, p 1
4. Massalski TB, Okamoto H, Subramanian PR, Kacprzak L (1990) Binary alloy phase diagrams, vol 2. ASM International, Materials Park, p 1444
5. den Broeder FJA, Nakahara S (1983) Scr Metall 17:399

6. Liu D, Miller WA, Aust KT (1989) Acta Metall 37:3367
7. Ma CY, Rabkin E, Gust W, Hsu SE (1995) Acta Metall Mater 43:3113
8. Kawanami Y, Kajihara M (1997) Netsushori 37:67
9. Kawanami Y, Nakano M, Kajihara M, Mori T (1998) Mater Trans JIM 39:218
10. Yamamoto Y, Uemura S, Kajihara M (1999) In: Proc int conf solid-solid phase transformations, Japan Inst. Metals, Kyoto, Japan, May 24–28, p 593
11. Yamamoto Y, Uemura S, Kajihara M (2001) Mater Sci Eng A 312:176
12. Yamamoto Y, Uemura S, Yoshida K, Kajihara M (2002) Mater Sci Eng A 333:262
13. Schwarz SM, Kempshall BW, Giannuzzi LA (2003) Acta Mater 51:2765
14. Yamamoto Y, Kajihara M (2008) J Electr Mater 37:1710
15. Massalski TB, Okamoto H, Subramanian PR, Kacprzak L (1990) Binary alloy phase diagrams, vol 2. ASM International, Materials Park, p 1455
16. Nakahara S, Abys JA, Abys SM (1983) Mater Lett 2:155
17. Chow KM, Ng WY, Yeung LK (1998) Surf Coat Technol 105:56
18. Bukaluk A (1999) Appl Surf Sci 144–145:395
19. Kuru Y, Wohlschlögel M, Welzel U, Mittemeijer EJ (2008) Thin Solid Films 516:7615
20. Chakraborty J, Welzel U, Mittemeijer EJ (2010) Thin Solid Films 518:2010
21. Kajihara M (2006) Scr Mater 54:1767
22. Yamamoto Y, Kajihara M (2001) Mater Trans 42:1763
23. Shewmon PG (1963) Diffusion in solids. McGraw-Hill, New York, p 14
24. Hartley GS (1931) Trans Faraday Soc 27:10
25. Darken LS (1948) Trans AIME 175:184
26. Metals Data Book (1993) Japan Inst Met (ed). Maruzen, Tokyo, p 21
27. Renouf TJ (1970) Philos Mag 22:359
28. Kaur I, Gust W, Kozma L (1989) Handbook of grain and interphase boundary diffusion data, vol 1. Ziegler Press, Stuttgart, p 363
29. Furuto A, Kajihara M (2008) Mater Trans 49:294
30. Hillert M (1986) In: Bennett LH (ed) Computer modeling of phase diagrams. TMS-AIME, Warrendale, p 1
31. Subramanian PR, Laughlin DE (1991) J Phase Equilib 12:231
32. Hartung F, Schmitz G (2001) Phys Rev B 64:245418
33. Baither D, Kim TH, Schmitz G (2008) Scr Mater 58:99
34. Kruse B, Baither D, Schmitz G (2010) Scr Mater 62:144
35. Schmitz G, Baither D, Kasprzak M, Kim TH, Kruse B (2010) Scr Mater 63:484
36. Li C, Hillert M (1981) Acta Metall 29:1949
37. Kajihara M, Gust W (1998) Scr Mater 38:1621
38. Hillert M (1999) In: Aaronson HI (ed) Lectures on the theory of phase transformations, 2nd edn. TMS-AIME, Warrendale, p 1
39. Nishikawa S (2001) Introduction to metallurgy. AGNE, Tokyo, p 530
40. Yamamoto Y, Kajihara M (1999) Acta Mater 47:1195
41. Yamamoto Y, Moriyama M, Kajihara M, Mori T (1999) Acta Mater 47:1757
42. Goukon N, Ikeda T, Kajihara M (2000) Acta Mater 48:1551